Japanese Journal of Applied Physics

The Japan Society of Applied Physics

REGULAR PAPER

Effects of post-annealing temperature and micropillar shape on physical properties of micropillar-type multiferroic composite thin films

To cite this article: Tsubasa Migita *et al* 2021 *Jpn. J. Appl. Phys.* **60** SFFB06

View the article online for updates and enhancements.

This content was downloaded from IP address 119.231.149.231 on 16/08/2021 at 06:57

Japanese Journal of Applied Physics **60**, SFFB06 (2021) **REGULAR PAPER**
https://doi.org/10.35848/1347-4065/ac1125

Effects of post-annealing temperature and micropillar shape on physical properties of micropillar-type multiferroic composite thin films

Tsubasa Migita[1*], Masafumi Kobune[1], Kengo Matsumoto[1], Yuuri Takeuchi[1], Hironori Fujisawa[2], Kensuke Kanda[2], and Kazusuke Maenaka[2]

[1]*Department of Chemical Engineering and Materials Science, Graduate School of Engineering, University of Hyogo, Himeji, Hyogo 671-2201, Japan*
[2]*Department of Electronics and Computer Science, Graduate School of Engineering, University of Hyogo, Himeji, Hyogo 671-2201, Japan*

[*]E-mail: en18g001@steng.u-hyogo.ac.jp

Received June 4, 2021; revised June 27, 2021; accepted July 4, 2021; published online July 23, 2021

Microplate (MP) and microrod (MR)-type $CoFe_2O_4$/$(Bi_{3.25}Nd_{0.65}Eu_{0.10})Ti_3O_{12}$ composite thin films were fabricated by a combination of reactive ion etching and metalorganic chemical vapor deposition. The effects of post-annealing temperature on the structural, magnetic, electrical, and magnetoelectric (ME) properties of the films were investigated. Based on the results, the optimal ferroelectric pillar structure to obtain a large ME voltage coefficient (α_{ME}) was determined. The electrical insulation properties for the films improved with increasing post-annealing temperature. On the other hand, magnetic and ferroelectric properties were degraded at high-temperature. Judging from the structural, magnetic, electric, and ME properties, the optimum post-annealing temperature was 700 °C. The shape of the ferroelectric layer had a significant influence on the ferroelectric properties and consequently on α_{ME}. The MR shape exhibited a smaller clamping effect than the MP shape, producing a greater ME effect. The α_{ME} for the MR-type film post-annealed at 700 °C was 5.5 mV cm^{-1} Oe^{-1}. © 2021 The Japan Society of Applied Physics

1. Introduction

Multiferroics (MFs) with both ferroelectric and ferromagnetic properties have attracted much attention. They are expected to be applied in a wide range of industries because they exhibit a magnetoelectric (ME) effect, which enables the electric polarization to be controlled by a magnetic field and the magnetism to be controlled by an electric field.[1–10] MFs can be roughly classified into single-phase and composite types. Most single-phase MFs exhibit ferroelectricity and ferromagnetism only at extremely low temperatures.[11] On the other hand, composite MFs exhibit both properties because they contain both a ferroelectric material and a ferromagnetic material, and are expected to produce a large ME effect at room temperature. Because of the increasing miniaturization of electronic devices, it is essential to use thinner materials to enable higher levels of integration. However, in the case of MFs, thinner films are affected by the clamping effect from the substrate, which suppresses the elastic interaction between magnetostriction and piezoelectric and prevents a large ME effect. Various thin-film structures have been studied in order to reduce this clamping effect,[12–14] and one such approach is the formation of pillars in the films. However, most such films are synthesized by self-assembled crystal growth, and there are many problems regarding their reproducibility and properties. Most studies on pillar-type films have investigated the use of a ferromagnetic material for the pillar structure and a ferroelectric material for the matrix. To date, there have been few reports on MFs with ferroelectric pillars and ferromagnetic matrices.[15] In our previous study, we have successfully fabricated *a*-axis oriented $(Bi_{3.25}Nd_{0.65}Eu_{0.10})Ti_3O_{12}$ (BNEuT) nanoplates with a unique nanoplate structure and large remanent polarization ($2P_r = 66\ \mu C\ cm^{-2}$) at room temperature.[16–18] The MF composite films were fabricated by utilizing the gaps in the nanoplate structure,[19,20] but the ME effect could not be clearly observed due to the small amount of ferromagnetic material introduced in the small gaps. Therefore, ferroelectric micropillar structure controlled sizes of gaps were fabricated by reactive ion etching (RIE). In this study, the micropillar obtained by line and space processing and grid processing are defined as microplate (MP) and microrod (MR) [Fig. 1], respectively. MP-type $CoFe_2O_4$ (CFO)/BNEuT(*h*00) composite thin films were successfully fabricated by densely depositing CFO in the MP gaps.[21] However, we have not been able to observe a clear ME effect. This is thought to be due to the small size of the deposited polycrystalline CFO particles, which results in a small elastic interaction between magnetostriction and piezoelectricity at the interface between the ferroelectric and ferromagnetic domain walls. In order to solve this problem and to obtain a clear ME effect, it is necessary to enhance the magnetostriction by increasing the grain size and controlling the orientation of the CFO film. In addition, there have been no reports on the effect of ferroelectric film geometry on the ME properties of MF composite thin films.

In this study, *a*-axis-oriented epitaxial BNEuT thin films were prepared by high-temperature sputtering followed by micropatterning using RIE to form MP and MR structures with a pitch size of 5 μm. Using these thin films as ferroelectric pillars, MP-type and MR-type MF composite thin films were subsequently deposited by metalorganic chemical vapor deposition (MOCVD). The effects of the post-annealing temperature on the structural, magnetic, electrical, and ME properties of the films were then investigated. Based on the results, we determined the optimal ferroelectric pillar shape to obtain a large ME voltage coefficient.

2. Experimental procedure

The *a*-axis-oriented epitaxial BNEuT thin films were fabricated by high-temperature sputtering on Nb:TiO_2(101) substrates using powder targets with a chemical composition of $0.7(Bi_{3.25}Nd_{0.65}Eu_{0.10})Ti_3O_{12} + 0.3Bi_2O_3$. MP and MR structures with a pitch size of 5 μm were fabricated by the same method as in our previous study.[22] CFO films were then deposited on the BNEuT(*h*00) MP and MR films by MOCVD using [Fe(*thd*)$_3$] as a Fe source and [Co(*thd*)$_2$] as a Co source. In order to confirm the effectiveness of the two pillar types, lamination-type CFO/BNEuT(*h*00) composite

 © 2021 The Japan Society of Applied Physics

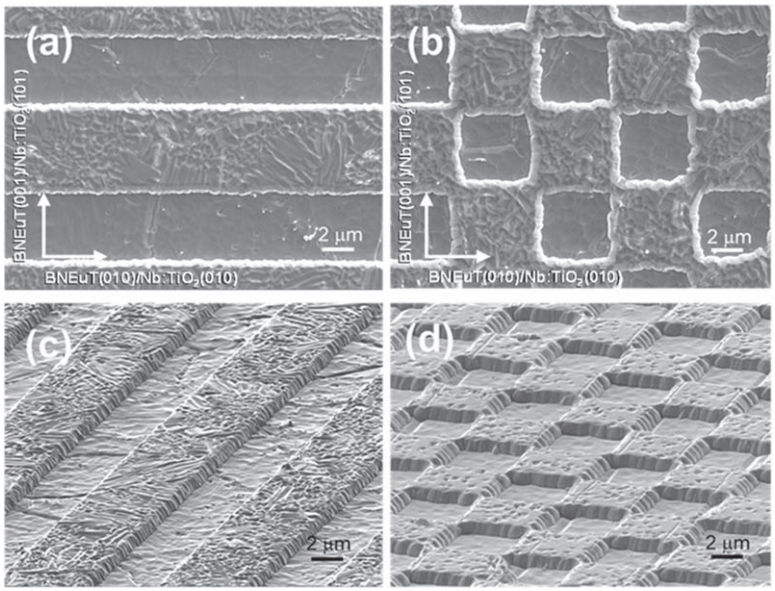

Fig. 1. Surface SEM images: (a) top view and (c) tilted view for MP-type film, and (b) top view and (d) tilted view for MR-type BNEuT film with a pitch size of 5 μm.

Table I. MOCVD conditions for CFO film on the BNEuT(*h*00)/Nb:TiO_2(101).

Metalorganic precursor	Fe(*thd*)$_3$	Co(*thd*)$_2$
Precursor temper. (°C)	145	111
Ar carrier gas flow rate (sccm)	109	100
Deposition pressure (Pa)	600	
Substrate temper. (°C)	550	
Deposition time (min)	140	
O_2 gas flow rate (sccm)	350	
Substrate	BNEuT(*h*00)/Nb:TiO_2(101)	

film was prepared under the same conditions. Table I shows the MOCVD conditions. The composite films were post-annealed at 600 °C–850 °C for 10 h under a nitrogen atmosphere.

Phase identification for the samples was conducted using X-ray diffraction (XRD; Rigaku Ultima IV) measurements at room temperature. The surface microstructure and Bi content for the films were investigated using a field-emission scanning electron microscopy (FE-SEM; JEOL JSM-7200F) system equipped with an energy dispersive X-ray spectrometry (EDS) detector. In-plane and out-of-plane room-temperature magnetization–magnetic field ($M-H$) characteristics were measured by applying a DC magnetic field in the range of 0 to ±5 kOe using a vibrating sample magnetometer (VSM; Toei Kogyo, VSM-5). The leakage current density −applied electric field ($J-E$) characteristics were measured at room temperature under an applied field that was swept from 20 to 400 kV cm^{-1} in 20 kV cm^{-1} steps, at 10 s intervals using a programmable electrometer (Keithley 617). Polarization−electric field ($P-E$) hysteresis loops were measured at room temperature using a ferroelectric test system (Toyo FCE3-EMS). The applied electric field and frequency were ±600 kV cm^{-1} and 100 Hz, respectively. The ME voltage coefficient (α_{ME}) was measured using a ME measurement system. A DC magnetic field and an AC magnetic field (δH_{AC}) were applied parallel to the sample surface at 0 to ±4.5 kOe and 10 Oe, respectively. The frequency of the AC magnetic field was 1 kHz. The obtained ME signal (δV) was measured using a lock-in amplifier (NF LI5640). The α_{ME} value was calculated using Eq. (1):[23]

$$\alpha_{ME} = \delta V / d \cdot \delta H_{AC}, \quad (1)$$

where δV, H_{AC}, and d indicate the ME voltage induced by the AC magnetic field, the applied AC magnetic field, and the thickness of the ferroelectric layer, respectively. The sample was poled by $P-E$ measurements repeated 50 times at an applied electric field of 600 kV cm^{-1} and a frequency of 100 Hz in advance.

3. Results and discussion

Figure 2 shows XRD profiles for MP-type CFO/BNEuT composite films with a pitch size of 5 μm post-annealed at 700 °C–850 °C and as-deposited films without post-annealing. Diffraction peaks indexed as 111, 311, 222, 400, 422, 511, and 440, which are attributed to the inverse spinel structure of CFO, were observed for all samples. On the other hand, new diffraction peaks indexed as 012, 110, and 024 attributed to hematite (α-Fe_2O_3), and 511 and 440 attributed to Co_3O_4 appeared at 800 °C–850 °C. These results indicate the thermal decomposition of CFO.[24]

Figure 3 shows surface FE-SEM images of MP-type films post-annealed at 700 °C–850 °C. With increasing post-annealing temperature, the average grain size increased in the range 237–503 nm. Particularly, at 750 °C–800 °C, the average grain size increased markedly from 259 to 438 nm. In general, a material with a low melting point binds particles with a high melting point, since the former becomes liquid first. In the present case, Bi has a melting point of 271 °C, Bi_2O_3 has a melting point of 820 °C, and CFO has a melting point of 1570 °C.[25] Noguchi et al. reported that Bi and O vacancies are formed in $Bi_4Ti_3O_{12}$ (BIT) crystals at high-temperature. In addition, it was reported that Bi (g), Bi_2O_3 (g), and O_2 (g) are generated as a result of defect formation in BIT at high-temperature.[26] Therefore, it is considered that volume and surface diffusion of Bi (g), Bi_2O_3 (g), and O_2 (g) in the upper CFO layer caused remarkable CFO grain growth in the post-annealing temperature range of 800 °C–850 °C.

© 2021 The Japan Society of Applied Physics

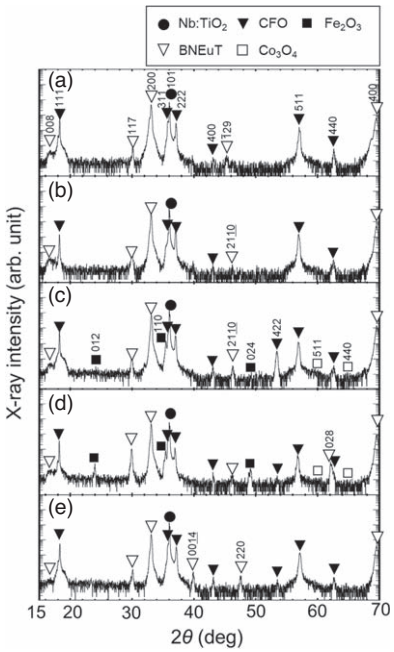

Fig. 2. XRD profiles for MP-type CFO/BNEuT composite films with a pitch size of 5 μm post-annealed at (a) 700 °C, (b) 750 °C, (c) 800 °C, and (d) 850 °C, and (e) as-deposited MP-type CFO/BNEuT composite film without post-annealing.

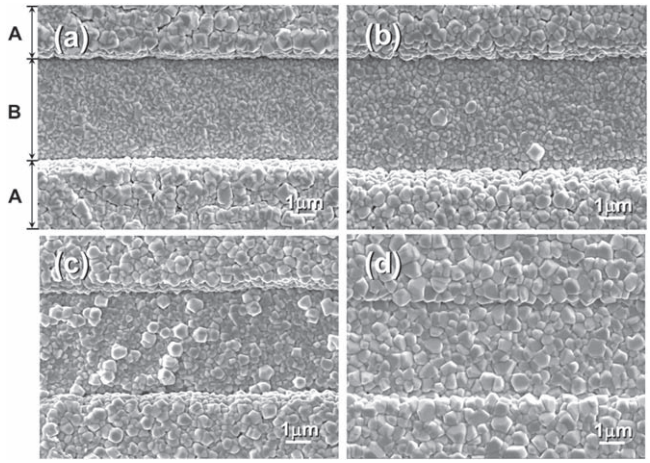

Fig. 3. Surface FE-SEM images of MP-type CFO/BNEuT composite films with a pitch size of 5 μm post-annealed at (a) 700 °C, (b) 750 °C, (c) 800 °C, and (d) 850 °C. A and B indicate the top and bottom parts of the line and space pattern, respectively.

Figure 4 shows in-plane and out-of-plane room-temperature $M-H$ hysteresis loops for MP-type films post-annealed at 700 °C–850 °C. The magnetization at 5 kOe ($M_{5\ \mathrm{kOe}}$) and remanent magnetization (M_r) in the in-plane direction are much larger than those in the out-of-plane direction. This suggests that this sample has shape magnetic anisotropy. Clear magnetic hysteresis loops were observed for the films post-annealed at 700 °C and 750 °C. The $M_{5\ \mathrm{kOe}}$ (46–49 emu g^{-1}) and the coercivity (H_c) (886–905 Oe) in the in-plane direction for the sample post-annealed at 700 °C–750 °C were superior to those for the as-deposited film ($M_{5\ \mathrm{kOe}} = 46$ emu g^{-1}, $H_c = 951$ Oe). On the other hand, a decrease in $M_{5\ \mathrm{kOe}}$ and H_c was observed in the in-plane magnetic hysteresis at 800 °C and 850 °C. In addition, the magnetic hysteresis loops had an unusual constricted shape.

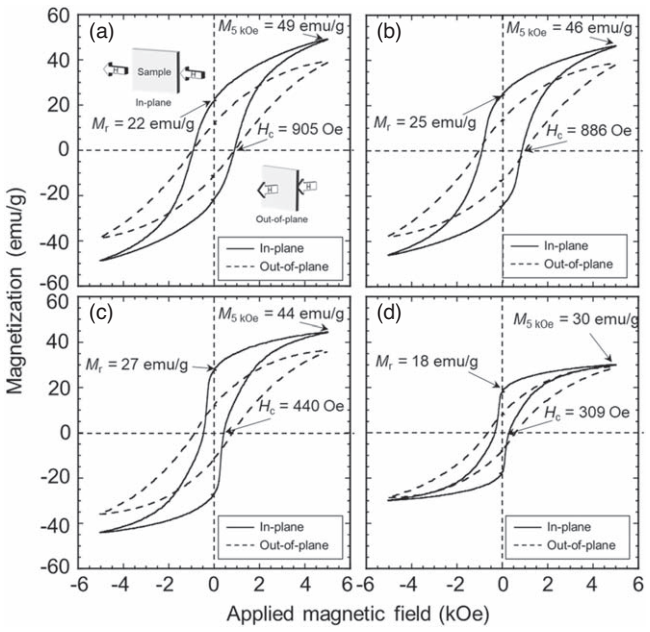

Fig. 4. Room-temperature in-plane and out-of-plane $M-H$ hysteresis loops for MP-type CFO/BNEuT composite films with a pitch size of 5 μm post-annealed at (a) 700 °C, (b) 750 °C, (c) 800 °C, and (d) 850 °C.

This is considered to be caused by the coexistence of antiferromagnetic α-Fe_2O_3[27] and Co_3O_4,[28] which appear as secondary phases with the main CFO phase, as is evident in the XRD patterns. Based on these results, a post-annealing temperature of 750 °C or lower is considered to be appropriate.

Figure 5(a) shows the $J-E$ characteristics of MP-type films post-annealed at 600 °C–850 °C. The leakage current density decreases significantly with increasing post-annealing temperature. The MP-type films post-annealed at 700 °C–850 °C showed excellent electrical insulation properties, with a leakage current density of less than 1.0×10^{-7} A cm^{-2} under an applied electric field of less than 100 kV cm^{-1}. In particular, the film post-annealed at over 800 °C maintained high electrical insulating properties (less than 5.4×10^{-7} A cm^{-2}) even under an applied electric field of 400 kV cm^{-1}. It is presumed that this is because the grain boundary volume of CFO, which acts as electrical conduction pathways, decreased due to the remarkable growth of CFO grains caused by high-temperature annealing. Figure 5(b) shows room-temperature $P-E$ hysteresis loops for MP-type films post-annealed at 600 °C–850 °C. Compared to the as-deposited film, P_r for the sample post-annealed at 600 °C was significantly reduced from 49 to 27 μC cm^{-2}. This is thought to be due to the reduction of leakage current by post-annealing, as shown in Fig. 5(a). For annealing temperatures of 800 °C and 850 °C, the loop shape became flattened in the transverse direction and the ferroelectricity was significantly reduced, despite the excellent $J-E$ characteristics. This may be attributed to the fact that polarization reversal was inhibited by the domain pinning associated with the formation of Bi and O vacancies in the underlying BNEuT layer during the high-temperature post-annealing process. Figure 5(c) shows the annealing temperature dependence of the Bi/Ti ratio and P_r value for MP-type films post-annealed at 600 °C–850 °C. The Bi content in the film decreased relatively slowly at 600 °C–650 °C, but significantly at

© 2021 The Japan Society of Applied Physics

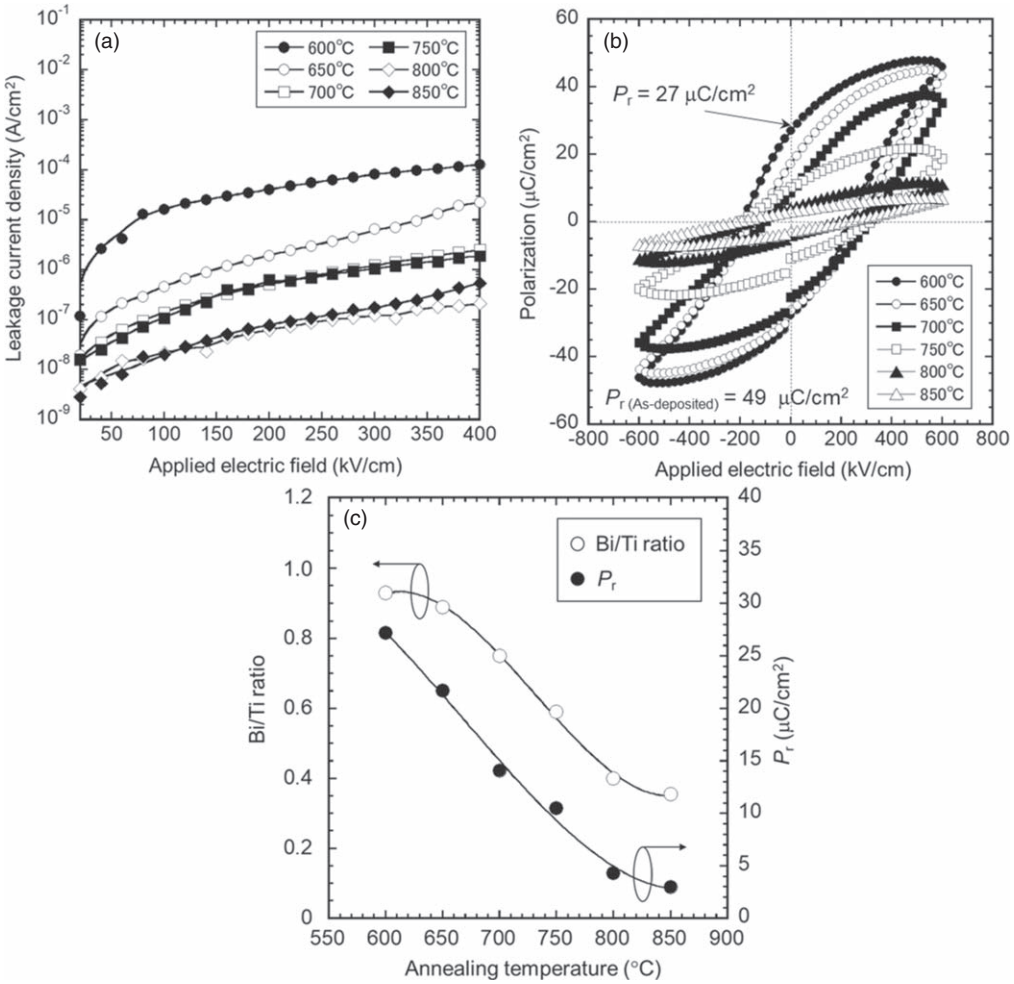

Fig. 5. (a) Room-temperature $J-E$ characteristics, (b) $P-E$ hysteresis loops, and (c) variations in the Bi/Ti ratio and P_r for MP-type CFO/BNEuT composite films with a pitch size of 5 μm post-annealed at 600 °C–850 °C. The Bi content was determined from the intensities of the Bi-Mα peak at 2.42 keV and the Ti-Kα peak at 4.51 keV in the EDS spectra.

650 °C–800 °C. This behavior is similar to that for P_r. These results demonstrate that evaporation of Bi occurs at high post-annealing temperatures, and as a result, the ferroelectricity of BNEuT decreases.

Figure 6(a) shows the room-temperature α_{ME} for MP-type films post-annealed at 600 °C–750 °C as a function of the DC magnetic field in the range of 0–4.5 kOe, which indicates ME behavior. This is similar to the ME behavior of lamination-type BIT/CFO composite film reported by Tang et al.[13] This confirms the occurrence of the ME effect in this material. However, the ME effect was not clearly observed for films annealed at 800 °C–850 °C. The reason for this is considered to be the decrease in magnetostriction due to the formation of antiferromagnetic α-Fe_2O_3 and Co_3O_4 by thermal decomposition of CFO, and the decrease in ferroelectricity due to the volatilization of Bi in the underlying BNEuT layer at high-temperature. The interaction between magnetostriction and piezoelectric is considered to have decreased due to the two factors described above. Here, the DC magnetic field at which α_{ME} shows a maximum is defined as H_{opt}. From the figure, H_{opt} shifts from the high field to the low field side with increasing annealing temperature from 600 °C to 750 °C. This may be explained as follows. The CFO layer (CFO $= 8.5 \times 10^{-6}$ °C^{-1})[29] is subjected to stress from the ferroelectric pillar layer (BIT-a-axis $= 4.7 \times 10^{-6}$ °C^{-1}, BIT-b-axis $= 12.3 \times 10^{-6}$ °C^{-1}, and BIT-c-axis $= 17.5 \times 10^{-6}$ °C^{-1})[30] due to the difference in the coefficient of linear expansion. Naturally, the degree of stress changes as the annealing temperature changes, and the magnetostriction behavior of the CFO thin-film layer is assumed to have been affected by the change.[31] Figure 6(b) shows the post-annealing temperature dependence of the maximum value of room-temperature α_{ME} for MP-type films. The α_{ME} increases at 600 °C–700 °C, reaches a maximum at 700 °C ($\alpha_{ME} = 2.1$ mV cm^{-1} Oe^{-1}), and then significantly decreases at 750 °C. The initial increase is due to the increase in magnetostriction caused by the increase in the grain size of CFO, which enhances the elastic interaction between magnetostriction and piezoelectricity. On the other hand, the subsequent decrease may be explained by the presumption that the effect of the decrease in ferroelectricity brought about by the volatilization of Bi in the BNEuT is greater than the effect of the increase in magnetostriction with increasing grain size. Based on these results, it is concluded that the optimum post-annealing temperature to obtain a maximum α_{ME} is 700 °C.

Figure 7(a) shows in-plane room-temperature $M-H$ hysteresis loops for MP-, MR- and lamination-type films post-annealed at 700 °C. All types showed good magnetic hysteresis. The magnetization for the lamination-type film is slightly smaller than that for the MP- and MR-type films, but there is almost no difference in M_r and H_c. This suggests that the magnetic properties are not affected by the shape of the underlying ferroelectric layer. Figure 7(b) shows $P-E$

© 2021 The Japan Society of Applied Physics

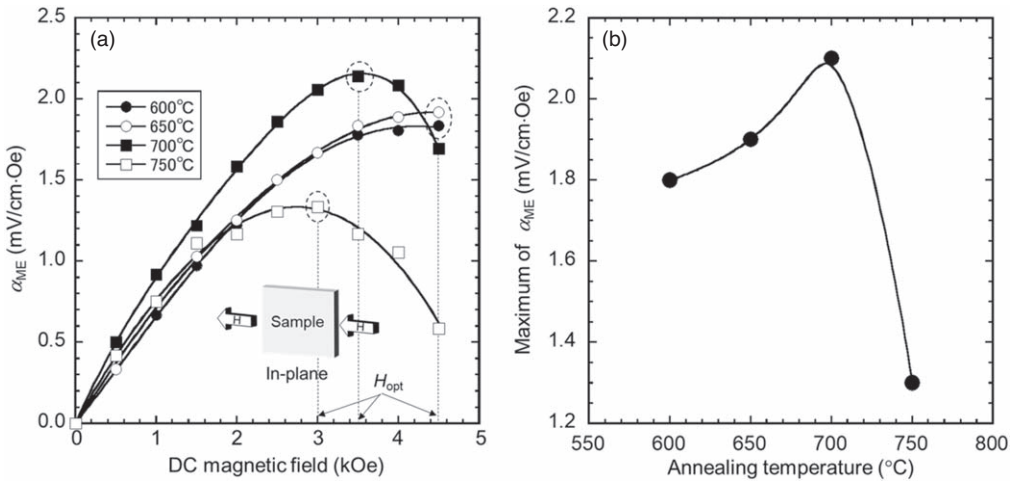

Fig. 6. (a) Room-temperature α_{ME} for MP-type CFO/BNEuT composite films with a pitch size of 5 μm post-annealed at 600 °C–750 °C as a function of the DC magnetic field in the range of 0–4.5 kOe, and (b) maximum room-temperature α_{ME} for the composite films as a function of annealing temperature in the range of 600 °C–750 °C.

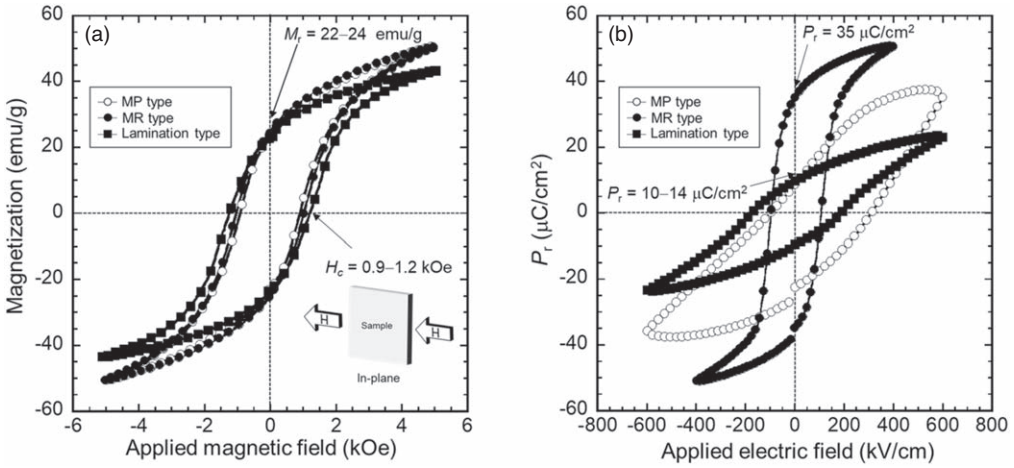

Fig. 7. (a) Room-temperature in-plane M–H hysteresis loops and (b) $P-E$ hysteresis loops for MP- and MR-type CFO/BNEuT composite films with a pitch size of 5 μm, and a lamination-type CFO/BNEuT composite film post-annealed at 700 °C.

hysteresis loops for the MP-, MR- and lamination-type films post-annealed at 700 °C. The $P-E$ loops for the MR-type film have a longitudinal rectangular shape with smaller E_c than those for the lamination- and MP-type films. The P_r ($=35\ \mu C\ cm^{-2}$) for the MR type is about 3.7 times larger than that for the lamination-type film and about 2.5 times larger than that for the MP-type film. This suggests that the clamping effect of the substrate is smaller for the MR-type film than for the MP- and lamination-type films.[32)]

Figure 8 shows α_{ME} for the MP-, MR-, and lamination-type films post-annealed at 700 °C as a function of the DC magnetic field in the range 0–4.5 kOe. The α_{ME}($5.5\ mV\ cm^{-1}\ Oe^{-1}$) for the MR-type film is 9.2 times larger than that for the lamination-type film and 2.6 times larger than that for the MP-type film. These results indicate that the shape of the underlying ferroelectric layer is closely related to α_{ME}. In other words, compared with the lamination-type film and the MP-type film, the MR-type film can suppress the clamping effect from the substrate to the lowest level and is effective for obtaining a large α_{ME}. This is presumably due to the fact that one MP is a continuous structure in one direction, while MRs are

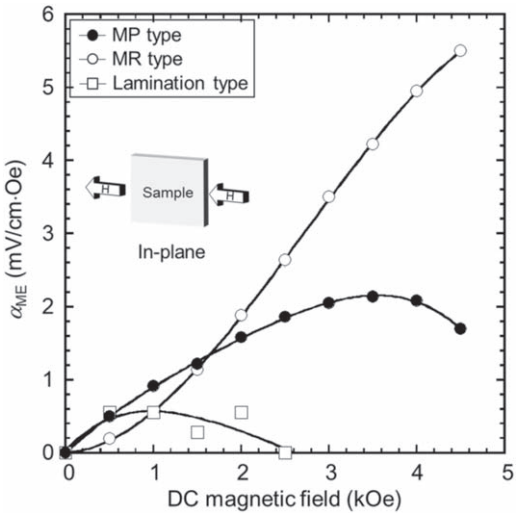

Fig. 8. Room-temperature α_{ME} for MR- and MP-type CFO/BNEuT composite films with a pitch size of 5 μm, and a lamination-type CFO/BNEuT composite film post-annealed at 700 °C as a function of the DC magnetic field in the range of 0–4.5 kOe.

© 2021 The Japan Society of Applied Physics

independent. In other words, the MR not only suppresses the constraint from the substrate but also reduces the constraint of the MR itself. From the viewpoint of the magnetic and ferroelectric properties, it can be concluded that the main reason for the dependence of α_{ME} on the shape of the ferroelectric layer is that the degree of clamping effect varies depending on the shape, and thus the ferroelectric characteristics change. We found that the MR-type film post-annealed at 700 °C shows the largest α_{ME} due to the small clamping effect. The α_{ME} (=5.5 mV cm^{-1} Oe^{-1}) of the MR-type composite film obtained in this study was smaller than that of the previously reported multilayer films of CFO/PZT (α_{ME} = 40–273 mV cm^{-1} Oe^{-1})[33,34] and CFO/BIT (α_{ME} = 29.3 mV cm^{-1} Oe^{-1})[13] due to various factors such as material properties and sample preparation method. However, if the MR structure is fabricated using a ferroelectric material with excellent piezoelectric constants such as PZT, an even larger α_{ME} than that of conventional multilayers can be expected.

4. Conclusions

MP-type and MR-type CFO/BNEuT composite films were fabricated and the effects of the post-annealing temperature and the ferroelectric layer morphology on their properties were investigated. The results can be summarized as follows:

(1) Judging from the structural, magnetic, electric, and ME properties, the optimum post-annealing temperature was 700 °C.
(2) The shape of the ferroelectric layer had a significant influence on the ferroelectric properties. The MR shape reduced the clamping effect and produced a large ME effect.
(3) The MR-type film post-annealed at 700 °C showed an α_{ME} value of 5.5 mV cm^{-1} Oe^{-1}.

Acknowledgments

This work was supported in part by a Grant-in-Aid for Scientific Research B (No. 18H01724) from the Japan Society for the Promotion of Science (JSPS).

ORCID iDs

Hironori Fujisawa https://orcid.org/0000-0002-8497-5846
Kensuke Kanda https://orcid.org/0000-0002-2395-120X

1) S. Dong, J. Zhai, F. Bai, J. F. Li, and D. Viehland, Appl. Phys. Lett. **87**, 062502 (2005).
2) J. Gao, Y. Wang, M. Li, Y. Shen, J. Li, and D. Viehland, Mater. Lett. **85**, 84 (2012).
3) D. R. Patil, Y. Zhou, J. E. Kang, N. Sharpes, D. Y. Jeong, Y. D. Kim, K. H. Kim, S. Priya, and J. Ryu, APL Mater. **2**, 046102 (2014).
4) J. Ryu et al., Energy Environ. Sci. **8**, 2402 (2015).
5) X. Yu, G. Lou, H. Chen, C. Wen, and S. Lu, IEEE Sens. J. **15**, 5839 (2015).
6) J. D. Schneider et al., J. Appl. Phys. **126**, 224104 (2019).
7) R. V. Petrov, A. S. Tatarenko, S. Pandey, G. Srinivasan, J. V. Mantese, and R. Azadegan, Electron. Lett. **44**, 506 (2008).
8) Y. Shen, J. Gao, L. Shen, D. Gray, J. Li, P. Finkel, D. Viehland, X. Zhuang, S. Saez, and C. Dolabdjian, Sensors Actuators A **171**, 63 (2011).
9) J. Das, J. Gao, Z. Xing, J. F. Li, and D. Viehland, Appl. Phys. Lett. **95**, 092501 (2009).
10) S. Dong, J. Zhai, J. F. Li, D. Viehland, and S. Priya, Appl. Phys. Lett. **93**, 103511 (2008).
11) T. Kimura, T. Goto, H. Shintani, K. Ishizaka, T. Arima, and Y. Tokura, Nature **426**, 55 (2003).
12) A. MacDannald, M. Staruch, G. Sreenivsulu, C. Cantoni, G. Srinivasan, and M. Jain, Appl. Phys. Lett. **102**, 122905 (2013).
13) Z. Tang, J. Chen, Y. Bai, and S. Zhao, Smart Mater. Struct. **25**, 085020 (2016).
14) H. Zheng et al., Science **303**, 661 (2004).
15) Y. Xu, J. F. Li, J. Ma, and C. W. Nan, J. Phys. D **45**, 315306 (2012).
16) M. Kobune et al., Jpn. J. Appl. Phys. **52**, 09KA10 (2013).
17) M. Kobune et al., Jpn. J. Appl. Phys. **53**, 02BC07 (2014).
18) M. Kobune, T. Kuriyama, R. Furotani, T. Kugimiya, S. Ueshima, T. Kikuchi, H. Fujisawa, S. Nakashima, M. Shimizu, and N. Fukumuro, Jpn. J. Appl. Phys. **54**, 10NA01 (2015).
19) M. Kobune, R. Furotani, S. Fujita, K. Kikuchi, T. Kikuchi, H. Fujisawa, M. Shimizu, and N. Fukumuro, Jpn. J. Appl. Phys. **55**, 10TA01 (2016).
20) K. Kikuchi, M. Kobune, T. Kikuchi, T. Migita, Y. Haruna, S. Yae, and N. Fukumuro, Trans. Mater. Res. Soc. Jpn. **43**, 105 (2018).
21) T. Migita et al., Jpn. J. Appl. Phys. **59**, SCCB10 (2020).
22) T. Obayashi, M. Kobune, T. Matsunaga, R. Ito, T. Migita, T. Kikuchi, K. Kanda, and K. Maenaka, Trans. Mater. Res. Soc. Jpn. **45**, 31 (2020).
23) G. V. Duong, R. Groessinger, M. Schoenhart, and D. B. Basques, J. Magn. Magn. Mater. **316**, 390 (2007).
24) M. Sugimoto, Denkikagaku **30**, 604 (1962) [in Japanese].
25) B. Purnama, A. T. Wijayanta, and Suhayana, J. King Saud Univ.-Sci. **31**, 956 (2019).
26) Y. Noguchi, M. Soga, M. Takahashi, and M. Miyama, Jpn. J. Appl. Phys. **44**, 6998 (2005).
27) R. Zysler, D. Fiorani, J. L. Dormann, and A. M. Testa, J. Magn. Magn. Mater. **133**, 71 (1994).
28) H. T. Zhu, J. Luo, J. K. Liang, G. H. Rao, J. B. Li, J. Y. Zhang, and Z. M. Du, Physica B **403**, 3141 (2008).
29) Y. Iwasaki, M. Kaneko, K. Hayashi, Y. Ochiai, M. Hayakawa, and K. Aso, J. Phys. E: Sci. Instrum. **22**, 498 (1989).
30) M. Kobune et al., Jpn. J. Appl. Phys. **49**, 09MA03 (2010).
31) A. E. Clark, M. W. Fogle, J. B. Restorff, and T. A. Lograsso, Mater. Trans. **43**, 881 (2002).
32) A. Bernal, A. Tselev, S. Kalinin, and N. B. Gharb, Appl. Phys. Lett. **101**, 112901 (2012).
33) Y. D. Xu, G. Wu, H. L. Su, M. Shi, G.-Y. Yu, and L. Wang, J. Alloys Compd. **509**, 3811 (2011).
34) Y. J. Eum, S. O. Hwang, J. Ryu, J. W. Kim, C. Y. Koo, J. Y. Lee, and H. Y. Lee, Ferroelectrics **465**, 76 (2014).

© 2021 The Japan Society of Applied Physics